

Targeted calibration to adjust stability biases in non-differentiable complex system models

Daniel Pals^{1*}, Sebastian Bathiany^{1,2}, Richard Wood³, Niklas Boers^{1,2,4*}

¹Technical University of Munich, School of Engineering and Design, Earth System Modelling,

Lise-Meitner-Straße 9, 85521 Ottobrunn, Munich, Germany

²Potsdam Institute for Climate Impact Research, Telegrafenberg A 31, Potsdam, 14473, Germany

³Met Office Hadley Centre, FitzRoy Road, Exeter, EX1 3PB, United Kingdom

⁴Department of Mathematics and Global Systems Institute, University of Exeter,

North Park Road, Exeter, EX4 4QE, UK

*Corresponding authors. E-mail: daniel.pals@tum.de and n.boers@tum.de

Numerical models of complex systems like the Earth system are expensive to run and involve many uncertain and typically hand-tuned parameters. In the context of anthropogenic climate change, there is particular concern that specific tipping elements, like the Atlantic Meridional Overturning Circulation, might be overly stable in models due to imperfect parameter choices. However, estimates of the critical forcing thresholds are highly uncertain because the parameter spaces can practically not be explored. Here, we introduce a method for efficient, systematic, and objective calibration of process-based models. Our method drives the system toward parameter configurations where it loses or gains stability, and scales much more efficiently than a brute force approach. We successfully apply the method to a simple bistable model and a conceptual but physically plausible model of the global ocean circulation, demonstrating that our method can help

find hidden tipping points, and can calibrate complex models under user-defined constraints.

Comprehensive numerical models of complex systems such as the Earth's climate are difficult to control because they are computationally expensive to run and depend on many free or at least uncertain parameters. Given the nonlinear dynamics typically represented by such models, they can respond to changes in these parameters in drastic and unforeseen ways. Such models are often not differentiable so that gradients of model output with respect to parameter changes cannot be computed. This makes systematic and objective parameter optimization impossible (1).

Prominent examples are climate and Earth system models (ESMs), which are highly costly numerical simulators of the Earth's climate, including general circulation models for the atmosphere and oceans, as well as land-surface, cryosphere, and carbon cycle components (2). Due to their complexity and the limited availability of observations, such models involve unavoidable and often unquantifiable uncertainties (3, 4). In particular, such models exhibit a large number, at the order of hundreds, of free parameters, e.g. from representing sub-grid scale processes that cannot be explicitly resolved, such as turbulent mixing, cloud formation, or biogeochemical phenomena.

Since state-of-the-art ESMs are not differentiable (1, 5), they are hand-tuned, instead of objectively calibrated. This tuning is performed based on subjective expert judgement, with the aim of approximately matching observed features like the global radiative balance or a target climate sensitivity (6–8). Moreover, even if an optimal choice of parameters may be found given an observational constraint, other relevant features of the climate system remain unconstrained, and a large part of the parameter space remains unexplored. In principle, such an exploration can be achieved with perturbed-physics ensembles (9) where a number of parameters is varied according to a pre-defined design, after which a simulation is performed for each parameter combination.

However, due to the often practically unquantifiable parametric uncertainty, and the structural uncertainty of any given model, these ensembles do not allow a probabilistic interpretation of the range of model outcomes (3, 4). Moreover, the large number of parameters and the large computational cost of running complex models prevents a thorough sampling of parameter space.

The existing parametric uncertainty of ESMs is problematic given the highly nonlinear dynamics of they describe, implying strong dependence even on small parameter variations. The resulting uncertainties are particularly severe in the context of so-called climate tipping points. These are

critical thresholds (e.g. in global mean temperature) where a component of the climate system may respond abruptly and reorganise into another state, potentially in an irreversible way (10–13). Such catastrophic phenomena can in some cases be associated with bifurcations in the underlying dynamics.

The most prominent elements of the Earth’s climate system that have been suspected to be able to show such tipping behaviour under anthropogenic forcing are the Atlantic Meridional Overturning Circulation (AMOC), the ice sheets on Greenland and Antarctica, and the Amazon rainforest (10, 11, 13). However, the associated critical forcing levels remain unconstrained mainly because of the large uncertainties in ESM simulations targeted at quantifying these thresholds. Current models do not show any robust agreement on such events in future projections (14). Moreover, there are reasons to believe that the above systems are overall too stable in ESMs compared to their real-world counterparts (15). This implies that undesired surprises could occur in the (near) future, which even the most sophisticated and comprehensive ESM projections cannot warn of. Methods to address existing stability biases in ESMs, and to identify plausible worst-case scenarios are therefore urgently needed.

A well-established framework for diagnosing stability changes from single trajectories relies on the phenomenon of critical slowing down (CSD) (11, 16, 17). When the linear stability of a stable equilibrium state is reduced and finally lost e.g. when reaching a bifurcation, the return time to equilibrium increases, and (assuming a continuous system at a fixed point) the largest negative eigenvalue increases toward 0. In addition, if the system is permanently perturbed by stationary noise, the autocorrelation of its state increases towards 1 (17, 18). CSD-based indicators have been found to increase in observations of a number of suspected climate tipping elements like the Greenland ice sheet (19) the AMOC (20), the Amazon rainforest (21, 22), or the South American monsoon (23). They have also been demonstrated to work in high-dimensional climate models (18, 24, 25), and have been successfully used to identify the perturbation pattern to which a system is least resilient (26–28).

Here, we present a CSD-based method to systematically and objectively adjust the stability of a given state of a simulated system. We do so by considering dynamics on the combination of the models phase and parameter space. As described in detail in the following, we create a feedback loop between the local stability of the system’s state and its parameter values. Based on a certain

initial state of the system and its parameters, our method determines the direction in parameter space where the system most effectively loses (or gains) stability under certain observational or physical constraints. Our general approach to this problem is to find a local parameter-dependent model which effectively describes the dynamics of an observable close to the stable state of interest, and then use this model to find a new parameter combination which increases or decreases the stability of the given equilibrium state. We note that our approach resembles many applications in control theory (29, 30), but with the target of altering the stability of the system, instead of keeping it in a functioning regime.

Using the CSD phenomenon makes our approach for targeted and objective model (re-)calibration highly efficient; as we will show below, our method scales polynomially with the numbers of parameters, whereas a brute-force approach would scale exponentially (the curse of dimensionality). This increase in efficiency is crucial in particular for non-differentiable models where gradients of model output with respect to parameter changes cannot be computed, as in the case for state-of-the-art climate and Earth system models (1, 5).

We describe our method in its most general way in the following section, and then apply it to two example systems, demonstrate its efficiency and discuss the implications of our results.

Targeted model calibration to adjust system stability

We consider a general dynamical system that is discrete in time, which essentially covers all numerical models of dynamical systems, including climate and Earth system models. We denote the dynamic variables (state variables) of the system by $\vec{x} \in \mathbb{R}^{d_x}$ and the parameters by $\vec{p} \in \mathbb{R}^{d_p}$. Moreover, we consider observables $\vec{o} \in \mathbb{R}^{d_o}$. We assume that we have access to a function $f_o : \mathbb{R}^{d_x+d_p} \rightarrow \mathbb{R}^{d_o}$, $(\vec{x}, \vec{p}) \mapsto \vec{o}$ mapping the state variables to the parameter-dependent observables (\vec{o}_t). As an example, motivated by the example of the AMOC, the system could be the global ocean circulation, and the observable the mass flux across a certain latitude in the North Atlantic.

The dynamics of the system is given in the form of an evolution function

$$f_p : \mathbb{R}^{d_x+d_p} \rightarrow \mathbb{R}^{d_x}, (\vec{x}_t, \vec{p}) \mapsto \vec{x}_{t+1},$$

which defines the one-step ahead propagation of the system state \vec{x}_t to \vec{x}_{t+1} and allows us to integrate

it. It is not necessary to know the exact expression of f_p ; we only need the ability to run parameter-dependent simulations of the system. We assume that the system's state fluctuates around a dynamic equilibrium which has a certain local stability, defined in terms of the linear restoring rate. The target is to adjust the system's parameters in a way that changes this local stability.

Our method consists of the following iterative steps (Fig. 1). For the sake of clarity, we focus on the case of destabilizing a given system; adjustments to the case of increasing stability are straightforward.

1. Generate a trajectory of observables (\vec{o}_t) of length T with parameters fixed to their initial values \vec{p}_{init} . To this end, we integrate the system to obtain a trajectory of the system variables (\vec{x}_t), to which we apply f_o . During the integration process we force the underlying system with additive noise $\vec{u}_t^{fixed} \in \mathbb{R}^{d_x}$ ("fixed" because the parameters are fixed here) in order to drive the system out of equilibrium and control the scale of the region in phase space used to compute the Jacobian at equilibrium.

$$\vec{x}_{t+1} = f_p(\vec{x}_t, \vec{p}_{init}) + \vec{u}_t^{fixed} \quad (1)$$

$$\vec{o}_t = f_o(\vec{x}_t, \vec{p}_{init}) \quad (2)$$

2. Fit a vector-autoregressive model (VAR(1) model) of the form

$$\vec{o}_{t+1} = \bar{v} + \bar{A}\vec{o}_t + \bar{\epsilon}_t^{fixed} \quad (3)$$

to the data from step 1. Since the equilibrium is stable, all eigenvalues of \bar{A} should be smaller than one and the stability of the system is characterized by the largest eigenvalue λ_{max} .

3. Vary the parameter values. To this end we use univariate autoregressive (AR(1)) processes of the form

$$p_{i,t+1} = (1 - \lambda_p) p_{i,init} + \lambda_p p_{i,t} + \sigma_i w_{i,t} \quad (4)$$

to generate a time series for each parameter p_i , fluctuating around $p_{i,init}$, where $(\vec{w}_{i,t})$ describes white noise with $w_{i,t} \sim \mathcal{N}(0, 1)$. Here we choose $\lambda_{max} \leq \lambda_p < 1$ such that the parameters vary on a time scale slower than the timescale of the system. This is necessary in order to record the response of the system to the parameter changes. In Sect. "Application to two example systems" we discuss how to choose appropriate noise amplitudes σ_i .

4. Further integrate the system, forcing it with the time-dependent parameter values:

$$\vec{x}_{t+1}^{vary} = f_p(\vec{x}_t^{vary}, \vec{p}_t) + \vec{u}_1^{vary} \quad (5)$$

$$\vec{o}_t^{vary} = f_o(\vec{x}_t^{vary}, \vec{p}_t) \quad (6)$$

Our aim is to learn from simulations what effect the parameter values have on the stability (and hence VAR parameters) of the system. We first try a naive approach by fitting a VAR(1) model of the form

$$\vec{o}_{t+1}^{vary} = \vec{\mu} + A_o \vec{o}_t^{vary} + A_p \vec{p}_t + A_{op} (\vec{o}_t^{vary} \otimes \vec{p}_t) + \vec{\varepsilon}_t^{vary} \quad (7)$$

with $A_o \in \mathbb{R}^{d_o \times d_o}$, $A_p \in \mathbb{R}^{d_o \times d_p}$, $A_{op} \in \mathbb{R}^{d_o \times (d_o \cdot d_p)}$ and the outer product

$$\vec{o} \otimes \vec{p} \equiv (o_1 p_1, o_1 p_2, \dots, o_1 p_{d_p}, \dots, o_{d_o} p_1, \dots, o_{d_o} p_{d_p})^T \in \mathbb{R}^{d_o \cdot d_p}, \quad (8)$$

where d_o is the number of observables and d_p the number of parameters.

In the above we keep second-order terms in order to detect the p-dependence of the eigenvalues (represented by Matrix \bar{A} in Eq. 3). If our trajectories only showed first-order dependencies on o and p, it would be possible to shift contributions between $\vec{\mu}$, A_o , A_p and A_{op} in Eq. 7, i.e., we would be faced with an underdetermined problem.

Moreover, if the magnitude of the variations of the observables \vec{o} and the parameters \vec{p} are not significantly smaller than the equilibrium values, second-order terms are hard to estimate even from long time series. In order to solve this problem, we compare the full VAR model to a model without parameter dependencies, making use of the knowledge of the noise trajectory ($\vec{u}_t^{(x)}$) that we used to force the dynamical system. The trajectory of the observable for the system with fixed parameters, (\vec{o}_t^{fixed}), is computed by

$$\vec{o}_{t+1}^{fixed} = f_o \left(f_p(\vec{x}_t^{vary}, \vec{p}_{init}) + \vec{u}_t^{(x)}, \vec{p}_{init} \right) \quad (9)$$

Assuming that the time evolution of the observables can indeed be described as suggested in equation 7, we obtain

$$\vec{o}_{t+1}^{vary} = \vec{\mu} + A_o \vec{o}_t^{vary} + A_p \vec{p}_t + A_{op} (\vec{o}_t^{vary} \otimes \vec{p}_t) + \vec{\varepsilon}_t^{vary} \quad (10)$$

$$\vec{o}_{t+1}^{fixed} = \vec{\mu} + A_o \vec{o}_t^{vary} + A_p \vec{p}_{init} + A_{op} (\vec{o}_t^{vary} \otimes \vec{p}_{init}) + \vec{\varepsilon}_t^{fixed} \quad (11)$$

Defining the time series $(\hat{o}_t) \equiv (\vec{o}_t^{vary} - \vec{o}_t^{fixed})$ we then find

$$\hat{o}_{t+1} = A_p \Delta \vec{p}_t + A_{op} (\vec{o}_t^{vary} \otimes \Delta \vec{p}_t) + \Delta \vec{\varepsilon}_t \quad (12)$$

with $\Delta \vec{p}_t \equiv \vec{p}_t - \vec{p}_{init}$ and $\Delta \vec{\varepsilon}_t \equiv \vec{\varepsilon}_t^{vary} - \vec{\varepsilon}_t^{fixed}$. If we now fit a VAR(1) model to the data $\vec{z}_t = \hat{o}_t$ and $Y_t = (\Delta \vec{p}_t^T, (\vec{o}_t^{vary} \otimes \Delta \vec{p}_t)^T)^T$ (see Methods, VAR(1) model estimation, for details of the notation) we can estimate A_p and A_{op} . Note that by using Y_t instead of y_t we assume $\vec{v} = 0$ in our estimation (see Methods). In the cases where we tested this method we obtained much better results for A_p and A_{op} compared to a naive approach.

Also note that this procedure is only possible when working with first-order VAR processes, which is the reason why we restricted ourselves to VAR(1) models only.

In order to also determine the missing coefficients from equation 7, we equate the VAR model from equation 3 to the model from equation 11, as both models describe the evolution for parameter values fixed to \vec{p}_{init} . By comparing coefficients, we obtain

$$\vec{\mu} = \vec{v} - A_p \vec{p}_{init} \quad (13)$$

$$A_o = \bar{A} - A_{op} (\text{Id}_{d_o} \otimes \vec{p}_{init}) . \quad (14)$$

A_p and A_{op} are given as estimated in step 4 above. The errors of the coefficients, as well as their correlations, can be computed using error propagation techniques. We consider the errors of both VAR estimations (i.e. the estimation for fixed and for varying parameters) as independent, since they arise from independent data.

5. Based on the estimated model from equation 7, we choose new parameter values. This step is quite problem-specific. The goal is to maximize the largest eigenvalue of $A_o + A_{op} (\text{Id}_{d_o} \otimes \vec{p})$, without allowing the eigenvalue to exceed 1, as we only aim at reducing the stability of the fixed point, and do not intend to make it fully unstable.

We also demand that the updated parameter values should not differ too much from the previous ones, as the model is only valid in a vicinity of these values. In addition, we preserve the mean values of the observables, which is equivalent to

$$\bar{o} \stackrel{!}{=} \vec{\mu} + A_o \bar{o} + A_p \vec{p} + A_{op} (\bar{o} \otimes \vec{p}) \quad (15)$$

with \bar{o} denoting the initial equilibrium values of the observables. This condition is problem-specific and motivated by the fact that the mean state (for example of the climate system) is typically constrained by observations much better than model parameters or the stability of the state. We will describe precisely how parameters were updated when applying our method in the next section.

6. After finding a new set of parameters, we replace \vec{p}_{init} by the new parameter values and run the system until it equilibrates. After that, the whole process is repeated, now using the new parameter values.

Application to two example systems

In order to test our method, we apply it to a simple double-well dynamical system, as well as to a conceptual, physically plausible model of the global ocean circulation (31) (see Methods).

Double-well system

We consider a simple double-well system with dynamics determined by the ODE

$$\dot{x} = p_1x^3 + p_2x^2 + p_3x + p_4 \quad (16)$$

For simplicity, we choose the observable o to be x itself, i.e. $f_o(x, \vec{p}) = x$. The deterministic part of the discretized system reads

$$x_{t+1} = x_t + dt \cdot (p_1x_t^3 + p_2x_t^2 + p_3x_t + p_4), \quad (17)$$

where we choose a time step of $dt = 10^{-3}$. We use the following initial parameter values:

$$\vec{p}_{init} = \begin{pmatrix} p_1 \\ p_2 \\ p_3 \\ p_4 \end{pmatrix} = \begin{pmatrix} -1 \\ 0 \\ 1 \\ 0 \end{pmatrix} \quad (18)$$

With this choice the system has two stable fixed points at $x = 1$ and $x = -1$ and one unstable fixed point at $x = 0$. Each fixed point has its own basin of attraction and the two basins are separated

by the unstable fixed point. We aim to destabilize the fixed point at $x = 1$ with regard to small perturbations in the x -direction whilst maintaining the position of the fixed point at $x = 1$.

As state noise, we add $\sqrt{dt} \sigma u_t$ to the right-hand side of the equation, with $u_t \sim \mathcal{N}(0, 1)$ and noise level $\sigma = 10^{-4}$. The resulting stochastic differential equation is then integrated using the Euler-Maruyama scheme.

We run the destabilization process for 18 iterations since further iteration would typically lead to a stochastic escape into the alternative basin of attraction.

The noise amplitudes used for the parameter variation are updated in each iteration step, as mentioned above. We calibrate these by first setting all noise amplitudes simultaneously to $10^{-3} \cdot \sqrt{1 - \lambda_p^2}$ and using these to compute varying parameter trajectories via equation 4. The system, forced by the varying parameters, is then integrated for 100 time steps. This is repeated iteratively whilst increasing the noise amplitudes in each iteration by a factor of 2, up to the point where the standard deviation of x exceeds a value of 10^{-3} . The noise amplitudes for generating the parameter series are then set to the values prior to the termination condition. To ensure that the VAR model actually shows a dependence on the parameter variations, we check whether the corresponding coefficients of the parameter-dependent VAR model significantly differ from zero, which was always the case (see Method section on noise amplitudes). With this method we typically find noise amplitudes corresponding to a standard deviation of the parameters (given by $\sigma_i / \sqrt{1 - \lambda_p^2}$ for parameter p_i) greater or close to 0.05. We also evaluate that the evolution of x is correlated to each of the parameters for the chosen noise amplitudes by checking whether the coefficients A_p and A_{op} significantly differ from zero (using the estimated errors on the coefficients).

We estimate the parameter-dependent VAR model using 1000 time steps for the fixed parameter model and 100 time steps for the parameter dependent part.

The parameters are then updated at the end of each iteration step by maximizing $A_o + A_{op}\vec{p}$ under the constraint of preserving the mean value $\bar{x} = 1$ i.e.

$$\bar{x} \stackrel{!}{=} \mu + A_o\bar{x} + A_p\vec{p} + \bar{x}A_{op}\vec{p}, \quad (19)$$

see equation 15. Using $\bar{x} = 1$ this equation is fulfilled if \vec{p} lies within the hyperplane defined by

$$\mathcal{H} = \{\vec{p} \in \mathbb{R}^{d_p} \mid \vec{n} \cdot \vec{p} = 1 - \mu - A_o\}, \quad (20)$$

$$\vec{n} \equiv \text{vec}(A_p) + \text{vec}(A_{op}). \quad (21)$$

We aim to destabilize the system, which corresponds to an increase of $A_o + A_{op}\vec{p}$. We hence choose a parameter update Δp of the form $\Delta p = \Delta\vec{p}_\perp + \lambda\Delta\vec{p}_\parallel$ with

$$\Delta\vec{p}_\perp = \frac{1 - \mu - A_o - \vec{n} \cdot \vec{p}_{init}}{|\vec{n}|^2} \vec{n} \quad (22)$$

$$\Delta\vec{p}_\parallel = \left[\text{vec}(A_{op}) - \frac{\text{vec}(A_{op}) \cdot \vec{n}}{|\vec{n}|^2} \vec{n} \right], \quad (23)$$

where $\lambda \in \mathbb{R}$. By adding $\Delta\vec{p}_\perp$ to \vec{p}_{init} , we move \vec{p} into the hyperplane in an orthogonal manner and $\Delta\vec{p}_\parallel$ is the orthogonal projection of $A_o + A_{op}\vec{p}$ into \mathcal{H} . Adding a multiple of $\Delta\vec{p}_\parallel$ to our parameter vector thus destabilizes the system without leaving \mathcal{H} . By then choosing

$$\lambda = \min \left(\frac{0.05}{|\Delta p_{\parallel,1}|}, \dots, \frac{0.05}{|\Delta p_{\parallel,4}|}, \frac{1 - A_o - A_{op}(\vec{p}_{init} + \Delta\vec{p}_\perp)}{2 \cdot A_{op}\vec{p}_\parallel} \right) \quad (24)$$

we assure by the first four arguments of the $\min(\dots)$ function – assuming that $|\Delta\vec{p}_\perp|$ is comparably small – that the parameter changes are not too large compared to the region explored in parameter space. The last term preserves the stability of the equilibrium at $x = 1$ by not pushing the value of $A_o + A_{op}\vec{p}$ past 1. To this end, we compute the value that λ would have to take in order for $A_o + A_{op}(\vec{p}_{init} + \Delta\vec{p})$ to be equal to one and use this value, divided by a factor of 2, as the last argument of the $\min(\dots)$ function.

The evolution of the updated parameters at the end of each iteration step is shown in Fig. 2a together with the evolution of the Jacobian λ , which indicates the stability of the equilibrium. Here, λ moving closer to 1 from below corresponds to a stability reduction of the system. The average value \bar{x} of x computed from a time series (obtained by integrating the stochastically forced system) consisting of 10^5 data points, using the parameter setting of the respective iteration step, can be successfully stabilised by our method (Fig. 2)b.

We notice that for the final iteration steps both λ as well as the parameter values start to converge in order to prevent the equilibrium from losing its stability entirely. This is a feature we explicitly implemented into the parameter update scheme by adding the last argument to the $\min(\dots)$ function in equation 24. Another striking aspect of Fig. 2 is that although the average value \bar{x} of x stays very close to its initial value in each iteration, there is a noticeable increase in fluctuations away from this value as λ approaches 1. The reason for this phenomenon likely lies in the fact that we did not change the amplitude of the noise $u_t^{(x)}$ added to the system; so as the stability of the fixed point decreases, the standard deviation of x and therefore also of \bar{x} increases.

The effect of the destabilization process to the RHS of equation 16 is visualized in Fig. 2c. The equilibrium at $x = 1$ is significantly destabilized while maintaining its original position. We note that the parameter change induced by our calibration method has shifted the other stable equilibrium, initially located at $x = -1$, to smaller values of x , while simultaneously increasing the size of the basin of attraction of that fixed point.

AMOC 5-box model

In order to test our method on a more complex, process-based system, we apply it to a recently proposed 5-box model of the overturning circulation of the global oceans (31). The model consists of five coupled differential equations describing the dynamics of the salinities in five boxes, where each box represents a water mass prevailing in a specific region of the Earth's oceans. We performed some slight modifications to the model regarding the conservation of total water mass (see Methods), which only have a negligible influence on the dynamics of the system. Here, the salinities $\vec{S} = (S_N, S_T, S_S, S_{IP}, S_B)^T$ are the system variables which we called \vec{x} in the previous section.

We select the AMOC strength q as our observable \vec{d} . We vary the parameters γ (the relative strength of a circulation branch involving the Southern Ocean), η (representing mixing of North Atlantic deep water with fresher waters), K_N , K_S and K_{IP} (representing diffusive fluxes associated with the gyre strengths in the North Atlantic, Southern Ocean and Indo-Pacific Ocean), as these five parameters have the largest uncertainties. The other parameters of the model are kept fixed at their original values.

We discretize the system with $dt = 0.1$ yr. The initial parameter values are chosen according to the FAMOUS_A model as stated by (31). We choose the additive noise driving the system such that the overall amount of salt in the system is conserved. To this end we add a random vector of the form

$$\vec{u}_t^{(x)} = \begin{pmatrix} u_t^{(1)}/V_N \\ u_t^{(2)}/V_T \\ u_t^{(3)}/V_S \\ u_t^{(4)}/V_{IP} \\ -(u_t^{(1)} + u_t^{(2)} + u_t^{(3)} + u_t^{(4)})/V_B \end{pmatrix} \quad (25)$$

with $u_t^{(i)} \sim \mathcal{N}(0, dt \cdot 10^{-8})$ to the salinity concentrations \vec{S}_t in each time step of the discretised model. We then ran the model for 500 iterations using 10^6 time steps (i.e. 10^5 years) in each iteration, for estimating the VAR model with fixed parameters (method step 2 above) as well as for finding the parameter dependencies of the model (step 4) in each iteration. Also, before starting the VAR estimation, we integrated the model for a transient time of 10^5 time steps (10,000 years) in each iteration to allow the model to equilibrate with the new parameter values. Due to their physical interpretation, the parameters are restricted to positive values and γ additionally must fulfill $\gamma \leq 1$ (though it turns out that imposing this condition is not necessary since the destabilization process decreases γ).

For calibrating the noise amplitudes σ_i , which are needed for generating the parameter series (cf. equation 4), we found that it is sufficient to calibrate each parameter separately. This helps determine the influence of any single parameter on the system. To this end, we fix all parameters but one to their initial values and iteratively increase the noise amplitude σ_i of the parameter of interest by powers of 2, starting from $\sigma_i = \min(10^{-5}, \vec{p}_{init,i}/4) \cdot \sqrt{1 - \lambda_p^2}$ up to the point where $\sigma_i / \sqrt{1 - \lambda_p^2} \in [5, 10]$. For each of these noise amplitudes we integrate the system for 10^{-5} time steps while forcing it only by the variations of p_i . From every such trajectory we then compute the variance $\text{VAR}(q)$ of our observable (the AMOC strength) and whether q shows a relationship to the varying parameter (by testing if coefficients are significantly different from zero as explained above). Out of all noise amplitudes which fulfilled both the causality condition and $\text{VAR}(q) < 0.01$, we selected the combination of noise amplitudes (one for each parameter) for which the corresponding values of $\text{VAR}(q)$ do not differ by more than a factor of 4 from each other. At the same time, the individual noise amplitudes are maximized in order to maximize the region which is explored in parameter space. To keep computational costs minimal, we only updated the noise amplitudes every 10 iteration steps.

After applying steps 1 to 5 from above, to find a model of the form

$$q_{t+1} = \mu + A_o q_t + A_p \vec{p} + q_t A_{op} \vec{p}, \quad (26)$$

we now systematically reduce the stability of the strong AMOC state in the 5-box model under a number of physical constraints, namely that $\Delta \vec{p}$ always stays on the same hyperplane, that no parameter value becomes negative, and that we stay sufficiently close to the region explored

in parameter space. The implementation of these constraints is explained in the corresponding Methods Section.

The parameter values and the observable state converge and are close to their final values after a few hundred iterations (Fig. 3a,b). From Fig. 3a we can also infer that both the parameters K_N and η have a major influence on the stability of the system, as they both rapidly tend towards zero within the first few iteration steps whilst simultaneously causing a significant decrease in the stability of the system.

These parameter values may be physically implausible; for example fresh water exchange by the wind-driven gyre circulation, represented by K_N , is known to be a stabilising factor, and observations and climate models show that this process is in operation in the North Atlantic (32, 33), suggesting that the minimum allowable value of K_N should be set somewhat greater than zero. Further, we have only used a single constraint on the destabilised equilibrium solution (the overturning strength q). We find that our destabilised equilibrium solution has box-mean salinities that are inconsistent with observations, in particular the box representing the Indo-Pacific oceans is too salty, while the boxes representing the North Atlantic and Southern Ocean are too fresh. Such additional observational constraints can in principle be added to our method, and would presumably result in a solution that is somewhat less unstable than the one we find here.

After destabilizing the five box model, we verify that its sensitivity to parameter changes in the form of freshwater forcing (so-called hosing) has increased. To this end, we apply freshwater hosing as described in (31) to both the original and the destabilized system (Fig. 3c-d). The effect of the parameter change induced by our method is similar to the one it had on the double well system: When exposed to the same hosing, the destabilized model (black lines in Fig. 3c-d) reaches an alternative steady state at much smaller hosing than the model with the original parameter values (red lines). Moreover, the negative hosing (reversed forcing) needed for the system to recover to its original state is much larger for the destabilized system, i.e. the regime with hysteresis has become wider (Fig. 3d).

Analysing the computational cost of the method

An important question regarding our calibration method for adjusting stability biases in complex system models is how well it performs in terms of computational cost when compared to a brute force parameter search. In particular, we are interested in how the computational cost scales with the number of parameters in our model.

Given a target stability of the dynamical system in question, the computational cost for finding a suitable parameter combination would scale exponentially with the number of adjustable parameters when applying a brute force parameter search. This manifestation of the so-called curse of dimensionality has so far prevented systematic calibration of climate or Earth system models, also because they are not differentiable. In the case of our method, the number of iterations needed to achieve the destabilization goal does not necessarily show any systematic dependency on the number of parameters, as the parameters evolve along a gradient of decreasing or increasing linear stability of the system. We therefore expect that the significant factor determining how the computational cost scales with the number of parameters will depend on how the length of the trajectory needed to estimate the parameter-dependent VAR model in each iteration step scales with the number of parameters. Since the length of such a trajectory would typically be independent of the number of parameters in a brute force setting, the main question is whether the length of the trajectory in an iteration step scales sub-exponentially.

We determine the scaling behavior of the trajectory length in the two example systems presented above. To this end, we consider each system with its respective initial parameter constellation. Then, in a first step, we only vary one parameter at a time, fixing all other parameter values. Using a trajectory of fixed length, we collect the errors on the coefficient A_{op} of the resulting VAR model for each separate parameter variation. This results in a vector $\sigma_{\text{one param. var.}}^2 \in \mathbb{R}^{d_p}$, where the i -th entry corresponds to the variances of A_{op} in a VAR model where only the i -th parameter is varied. The reason why we only focus on the error of A_{op} , as opposed to also considering further coefficients, is due to simplicity and the fact that A_{op} is the most relevant coefficient for parameter updates when purely aiming for a change in stability.

In a second step, we iterate through all possible parameter constellations including at least two parameters. For each such parameter set we iteratively increase the trajectory length used to

compute a VAR model in each iteration, and compare the variance of the sum of all entries of A_{op} (taking correlations into account) of the resulting VAR model to the sum of the respective entries in $\sigma_{\text{one param. var.}}^2$. As soon as the variance of the sum of A_{op} entries drops below the latter sum, the current trajectory length necessary to fulfill this condition is noted. The reason why we do not directly compare the variances of each coefficient in A_{op} to its counterpart in $\sigma_{\text{one param. var.}}^2$ is that this can lead to extremely long trajectory lengths necessary to meet this condition, in the case that the entries in $\sigma_{\text{one param. var.}}^2$ differ in magnitude. Thus, if the total number of parameters that can possibly be varied is given by d_p and the currently considered set of parameters consists of p parameters, this results in $\binom{d_p}{p}$ trajectory lengths, corresponding to the case of p parameters being varied. By averaging over all values corresponding to a given value of p and visualizing this data, we can try to infer the functional dependence of the trajectory length with regard to the number of parameters being varied.

For each given parameter set, we always use the same noise amplitudes σ_i for a given parameter p_i regardless of the other parameters it is paired up with. In the case of the double-well system we used $0.05 \cdot \sqrt{1 - \lambda_p^2}$ as noise amplitude for every parameter. For the 5-box AMOC model we used $(\sigma_\gamma, \sigma_\eta, \sigma_{K_N}, \sigma_{K_S}, \sigma_{K_{IP}}) = (0.020, 5.243, 0.328, 0.082, 2.621) \cdot \sqrt{1 - \lambda_p^2}$, where we determined the noise amplitudes utilizing the procedure described above (AMOC 5-box model). As this choice of noise amplitudes for the 5-box model led to quite long trajectory lengths necessary to fulfill the convergence condition, we also empirically modified the noise amplitudes to be $(\tilde{\sigma}_\gamma, \tilde{\sigma}_\eta, \tilde{\sigma}_{K_N}, \tilde{\sigma}_{K_S}, \tilde{\sigma}_{K_{IP}}) = (0.020 \cdot 32, 5.243/32, 0.328/2, 0.082 \cdot 2, 2.621/8) \cdot \sqrt{1 - \lambda_p^2}$, which resulted in much shorter trajectory lengths. We will refer to the resulting model as the optimized box model system in the following.

When determining the values of $\sigma_{\text{one param. var.}}^2$ we used VAR models computed from data series of length 6000 in the case of the double well system and length 1000 for the two 5-box model versions. In order to suppress stochastic effects we repeated this procedure 100 times and took the final value of $\sigma_{\text{one param. var.}}^2$ to be the average over all of these runs. For each parameter set including at least two parameters, we computed the trajectory length needed to fulfill the condition described above as the average over 20 such runs. To this end we increased the trajectory length by 1000 in each iteration step, starting from 6000 for the double well system and from 6000 for the optimized

5-box model system). For the non-optimized 5-box model we increased the trajectory length in the following fashion: $10^3, 2 \cdot 10^3, 5 \cdot 10^3, 10^4, 2 \cdot 10^4, 5 \cdot 10^4, 10^5, \dots$ in order to save computation time.

The results of the analysis concerning the computational cost of the method are shown in figure 4. We notice that the data, displayed in a log-log plot, agrees well with respective linear fits. One can also observe that the range of trajectory lengths which we observe for parameter subsets with a fixed number of parameters (small data points), decreases as this number grows in all three cases.

Discussion

In both examples that we considered, namely the simple double-well system and the 5-box model of the global ocean circulation, our method was able to adjust the stability of the modelled system. Specifically, focusing on the task of reducing stability, the largest eigenvalue λ was pushed closer to 1. The computational cost when destabilising the double well system as well as the five box model shows a polynomial dependency on the number of parameters under consideration, although the leading order power seems to differ between the two models (Fig. 4). This polynomial dependency implies great improvement of our method compared to a brute force parameter search. This is particularly relevant for non-differentiable models such as state-of-the-art comprehensive climate and Earth system models, where gradients of model output with respect to parameter variations cannot be computed. Yet, brute-force approaches are prohibitive due to the enormous computational costs of running these models, leaving subjective manual tuning as only option so far.

We note that our method is not designed to find the most unstable version of the system. Since the result depends on the specific initial conditions of the system state and parameters, its purpose is to efficiently approach regional minima of the stability landscape. In order to scan larger regions in parameter space, global methods have been designed. For example, one can perform perturbed-physics ensemble simulations (9), where model parameter combinations are chosen by a Latin Hypercube sampling (34), and then use Gaussian process emulators to interpolate between the chosen points in parameter space, optionally also discarding realisations that are in contradiction to physical principles or observations (35, 36). Such global approaches and our local optimisation method are complementary approaches, which may be combined in a novel way to illuminate a model's dependency on parameters in a global way. In cases where more physical or observational

constraints are applied to the parameter ranges and the resulting equilibrium solutions than we used here, the resulting target region of parameter space may already be rather constrained, and our local search method may indeed already deliver a global optimum by itself.

The largest challenge associated with applying our method is that it can be difficult and computationally expensive to find suitable hyper parameters, involving the calibration of the amplitudes of the noise imposed on the system state or the parameters, or the choice of suitable observables. In general, the final parameter configuration can potentially depend on the choice of these hyperparameters. Depending on how we choose the observables and the state noise, our method offers flexibility as to which aspects the system is stabilized or destabilized (through the choice of observables) and also what type of perturbations are relevant (by choosing suitable noise).

The methods we used for the respective examples as explained in the main text are procedures we found to work well for the respective systems. There is no guarantee that they are optimal for other simulated systems. However, we also propose a number of additional methods to evaluate the quality of the VAR model fit (SI, first section), to test the whiteness of the residuals (SI, second section), and an approach for improving the VAR estimation by denoising (SI, third section). We implemented and applied the latter method to our two example systems, which yielded similar results to those discussed above. While we expect these extended approaches to work in general, application-dependent procedures may be more efficient in specific cases.

The fact that the result depends on the constraints on the parameter values is a desired property. For example, parameters in ESMs are often constrained by observations or by their physical meaning. Considering the 5-box model, we notice that even after 500 iteration steps we were not able to push λ as close to 1 (Fig. 3b) as in the case of the double well system. This is likely due to the fact that some parameters hit the boundaries of their restricted ranges (they become zero, see Fig. 3a), which might prevent the system from reaching an arbitrary degree of destabilization. Due to the possibility to combine our method with domain-specific constraints, and pick observables relevant in the real world, it can potentially be beneficial in exploring a range of climate change trajectories that are all constrained by observations and theory, but reveal worst-case scenarios in terms of climate tipping points.

An indicator for potential improvements lies in the convergence of the tuned parameter values. In general, each parameter has a clear tendency for the system to lose stability, despite the stochastic

elements in our approach. We see an exception to this within the first ~ 50 iteration steps for the 5-box model, where some parameters seem to evolve contrary to their overall tendency (Fig. 3a). This effect seems to be correlated with the average value \bar{q} of q significantly deviating from its target value. A possible explanation could be that at this point the VAR model does not extrapolate well, causing parameter changes to affect the system in an unforeseen way. On one hand, this issue could be fixed by temporarily and adaptively decreasing the step size of the parameter updates between iteration steps. On the other hand, this is not required as long as q recovers back to its original value after a temporary anomaly. Moreover, the fixed step size reduces the computational cost of our method.

Our method is flexible in the requirements that one imposes on the updated parameter values, which in general could

- preserve the equilibrium values of the observables by fulfilling equation 15.
- only take on allowed values in case the parameters are restricted.
- not exceed a certain step change, which would typically depend on the noise amplitudes σ_i used for the parameter variation as these determine the explored region in parameter space.
- minimize the errors of the new value of the maximal eigenvalue or the error on the accuracy on how well the condition for preserving the observable values is fulfilled.

All of these conditions (and possibly more) can be included in the parameter update by either implementing these as constraints or as penalty terms in the optimisation problem that needs to be solved in order to determine the new parameter values.

Further research on this topic could be dedicated to applying our method to more complex models and finding more efficient ways for determining appropriate hyper-parameter values. Also, a more detailed investigation on how the computational efficiency scales with the number of parameters compared to brute force methods, could be of great interest. Moreover, instead of fitting VAR models to the simulated time series, Machine Learning approaches (30, 37, 38) may also be useful to achieve for targeted calibration to adjust stability.

Our implementation of the method is fully automated, i.e. all steps outlined above, including the noise calibration and iterative parameter updates, work without intervention. In principle, it is

straightforward to apply our method to more complex models, though the parameter updates would require including the compilation of the model code into the procedure. A more fundamental caveat can be that the "noise level" of the observables cannot be directly controlled in complex models such as comprehensive ocean or atmosphere general circulation models, where apparent stochasticity emerges from the chaotic internal dynamics on short time scales. The fixed point stability of the slower dynamics may then not be perfectly sampled, e.g. due to multiplicative and / or large noise.

Regarding the large parametric uncertainty of comprehensive ESMs and the large cost of running a single simulation, our method can still demand an unfeasible simulation time when applying it to state-of-the-art ESMs. A major limitation here is the typical timescale of the problem under consideration, perhaps even more so than the number of perturbed parameters. In the case of the ocean circulation, this can require time series of many thousands of years. In other cases however, e.g. regarding the parameterisation of interactions between the land surface and the atmosphere, the applicability to some complex ESMs is within reach. Moreover, our method may also be applied to statistical emulators of complex numerical models (34, 39), or process-based reduced-complexity models (40). Specifically, the 5-box ocean circulation model in our example has been informed by more complex models and physical understanding in its construction and parameterisations (31). We propose that climate scientists should aim for meaningful model hierarchies and use automated calibration as proposed here as a means to tighten the relationship between the models of the hierarchy, in order to learn something about the stability of more complex climate models and the real world.

Due to its flexibility regarding the purpose of the model, the nature of the constraints, and the target property to be optimised, our method is not restricted to applications with the goal of varying the stability of dynamical systems, but can potentially be applied to a wide class of optimisation problems within the context of complex dynamical systems.

Conclusion

We have introduced a targeted method for systematic and objective parameter calibration to adjust system stability in non-differentiable complex system models, under given physical and observational constraints. Our method considers dynamics on the combination of a given model's phase

and parameter space and exploits the the phenomenon of CSD to identify the optimal direction in parameter space to adjust the stability of modelled systems in a desired way. This makes the method computationally highly efficient, breaking the curse of dimensionality by scaling only polynomially in the number of parameters. Our results are particularly promising given the persisting concerns that major Earth system components are too stable in state-of-the art climate and Earth system models, which are very challenging to calibrate objectively.

Materials and Methods

VAR(1) model estimation

We assume a general setting in which we are given two time series (\vec{z}_t) and (\vec{y}_t) with $t \in \{0, \dots, T\}$, which can potentially be identical. Our goal is to find a model of the form

$$\vec{z}_{t+1} = \vec{v} + A\vec{y}_t + \vec{\varepsilon}_t \quad (27)$$

which fits the data best in the sense of a least square estimate concerning the error vectors $\vec{\varepsilon}_t$.

In order to provide compact formulas we introduce the notation

$$Z = (\vec{z}_1, \dots, \vec{z}_T) \quad (d_z \times T) \quad (28)$$

$$Y_t = \begin{pmatrix} 1 \\ \vec{y}_t \end{pmatrix} \quad ((d_y + 1) \times 1) \quad (29)$$

$$Y = (Y_0, \dots, Y_{T-1}) \quad ((d_y + 1) \times T) \quad (30)$$

$$E = (\vec{\varepsilon}_1, \dots, \vec{\varepsilon}_T) \quad (d_z \times T) \quad (31)$$

$$B = (\vec{v}, A) \quad (d_z \times (1 + d_y)) \quad (32)$$

where d_z and d_y are the dimensions of \vec{z}_t and \vec{y}_t respectively. We then find (also see Eq. (3.2.10) in (41)) that the unbiased least square estimate for B is given by

$$B = ZY^T(Y Y^T)^{-1} \quad (33)$$

Further we also get an unbiased estimate for the covariance matrix of the error terms $\vec{\varepsilon}_t$ given by

$$\Sigma_\varepsilon = \frac{1}{T - d_y - 1} Z \left(I_T - Y'(Y Y^T)^{-1} Y \right) Z' \quad (34)$$

as described in Eq. (3.2.19) in (41).

In order to give an expression of the errors and correlations of the coefficients in B we introduce

$$\vec{\beta} = (B_{1,1}, B_{2,1}, \dots, B_{d_z,1}, \dots, B_{1,1+d_y}, \dots, B_{d_z,1+d_y})^T \quad (35)$$

The covariance matrix of $\vec{\beta}$ (for asymptotically large T) can then be estimated as

$$\Sigma_{\beta} = \frac{\left(\frac{YY'}{T}\right)^{-1} \otimes \Sigma_{\varepsilon}}{T} \quad (36)$$

which can be found in section 3.2.2. of (41).

We also estimate the errors of the coefficients by using $(\vec{z}_t) = (\vec{o}_t)$ and $(\vec{y}_t) = ((\vec{o}_t^T, \vec{p}_t^T, \vec{o}_t^T \otimes \vec{p}_t^T)^T)$. We make use of these errors when calibrating the noise amplitudes in order to test the dependence of the observables on the varying parameters, by checking whether the VAR coefficients significantly differ from zero.

Finding appropriate noise amplitudes for the parameter variation

The task of choosing the noise amplitudes σ_i when generating the parameter series as presented in equation 4 is rather problem-specific, as one has to find a satisfactory trade-off between the importance of well chosen noise amplitudes and the time it takes to compute these. Quality features of well chosen noise amplitudes would be that the respective coefficients of A_p and A_{op} from Eq. 7 significantly differ from zero while having small errors. Moreover, the noise amplitude should not be too large, i.e. no restrictions on the parameter ranges should be violated during the parameter variation process and the overall structure of the dynamical system (close to the considered equilibrium) should, of course, remain preserved. A possible indicator for quantifying whether the parameter variation disturbs the system too much is given by the variances of the observables when integrating the system with varying parameters. A possibility for checking if the respective coefficients of A_p and A_{op} indeed significantly differ from zero when considering a given parameter p_i is presented in the following (also see section 3.6 in (41)):

Let C be a $(n \times d_x(d_y + 1))$ matrix such that $C\vec{\beta}$ only consists of the n coefficients in $\vec{\beta}$ that are relevant for the coupling of the parameter under consideration to \vec{o} . Then we can compute the

following statistic

$$\lambda_F = \frac{1}{n} (C\vec{\beta})' [C((YY')^{-1} \otimes \hat{\Sigma}_\varepsilon)C']^{-1} C\vec{\beta} \quad (37)$$

which we expect to follow an $F(n, T - d_y - 1)$ -distribution in the case that there is no causal relationship from \vec{p} to \vec{o} .

In a more simplified procedure, one can alternatively check if any of the relevant coefficients significantly differ from zero using the estimated errors for these coefficients. This is what we used for both the AMOC and the double-well system. In order to find suitable noise amplitudes, possible approaches could include grid searches or more sophisticated methods where the noise amplitudes are simultaneously varied until certain conditions are met (cf. the procedure described for the double well system). Alternatively, one could find an optimal noise amplitude for each parameter separately and hope that these then also work well together, by choosing a combination of amplitudes where the variances of the observables lie on comparable scales for each separate parameter variation, as we did for the AMOC system. Also note that for most systems it might not be necessary to update the noise amplitudes in each iteration which can save computational costs.

Constraints used when destabilising the 5-box model

In order to destabilise the 5-box model under certain constraints, we define

$$\vec{n} \equiv A_p + \bar{q}A_{op} \quad (38)$$

$$u \equiv \bar{q}(1 - A_o) - \mu - \vec{n} \cdot \vec{p}_{init} \quad (39)$$

$$\vec{v} \equiv \text{vec}(A_{op}) \quad (40)$$

where \vec{n} is the normal vector to the hyperplane spanned by \vec{p} , and \vec{v} is the gradient of the quantity we want to optimize (with derivative w.r.t. \vec{p}), \bar{q} is the equilibrium value of the AMOC strength that we desire to preserve. With this notation, the quantity we maximize is $\vec{v} \cdot \Delta\vec{p}$, where $\Delta\vec{p}$ again denotes the change in the parameter values during the parameter update. The condition of keeping the equilibrium value of q at \bar{q} can now be written as

$$u \stackrel{!}{=} \vec{n} \cdot \Delta\vec{p} \quad (41)$$

We computed $\Delta\vec{p}$ by maximizing

$$M \equiv \vec{v} \cdot \Delta\vec{p} - \eta_1(\vec{n} \cdot \Delta\vec{p} - u)^2 - \eta_2(\Delta\vec{p}^T, -1, 0, \dots, 0)\Sigma_{nuv} \begin{pmatrix} \Delta\vec{p} \\ -1 \\ 0 \\ \vdots \\ 0 \end{pmatrix} - \eta_3(0, \dots, 0, \Delta\vec{p}^T)\Sigma_{nuv} \begin{pmatrix} 0 \\ \vdots \\ 0 \\ \Delta\vec{p} \end{pmatrix} \quad (42)$$

under the constraint

$$l^2 \doteq \sum_i \frac{\Delta p_i^2}{l_i^2} \quad (43)$$

Here, Σ_{nuv} denotes the correlation matrix of $(\vec{n}^T, u, \vec{v}^T)^T$ which can be computed from Σ_β (cf. equation 36) using error propagation and l is the prescribed length of $\Delta\vec{p}$ with regard to a metric determined by the parameter-dependent weights l_i . We here set l to 100 and used

$$l_i = \min\left(\frac{\sigma_i}{\sqrt{1 - \lambda_p^2}}, \frac{p_{init,i}}{100}\right) \quad (44)$$

with σ_i and λ_p from equation 4. With this choice we guarantee that no parameter value becomes negative and that we stay sufficiently close to the region explored in parameter space.

To summarise the above equations, we update the model parameters \vec{p} under different constraints by looking for the change in parameters with fixed length l (in the metric l_i , Eq. 44), while maximizing $\vec{v} \cdot \Delta\vec{p}$ under the additional condition that \vec{p} must stay within the hyperplane. In contrast to the approach used for the double-well system, we achieve this by adding a very high penalty term (term with η_1 in Eq. 42) to account for this condition.

Essentially, l_i measures how large the explored region is for parameter p_i . We rescale all parameters by their respective exploration range in order to make them comparable and then demand that the Euclidean norm of this rescaled parameter vector must equal 100.

The terms involving η_2 and η_3 in Eq. 42 penalize the uncertainties on how $\vec{v} \cdot \Delta\vec{p}$ and the first penalty term (η_1 term) change for a parameter update by $\Delta\vec{p}$. Thus, these last two terms in Eq. 42 assure that with a high probability our parameter update indeed has the desired effect of stabilizing or destabilizing the system and preserving the AMOC strength. The trade-off for this is that the destabilization process could potentially become less efficient. We set the penalty coefficients to $\eta_1 = 10^{12}$, $\eta_2 = 10^3$ and $\eta_3 = 1$, where the first penalty term penalizes the distance of $\Delta\vec{p}$ to the hyperplane determined by \vec{n} and u , the second term penalizes the error on $\vec{n} \cdot \Delta\vec{p} - u$, and the third term penalizes the error on $\vec{v} \cdot \Delta\vec{p}$.

The 5-box AMOC model

The model represents the meridional global ocean circulation ("global conveyor belt") in the form of five boxes. The model has been designed to represent the Atlantic Meridional Overturning Circulation (AMOC), and its connected major circulation features on the globe (31, 42). The set of equations we use is:

$$q = \frac{\lambda}{1 + \lambda\alpha\mu} [\alpha(T_S - T_0) + \beta(S_N - S_S)] \quad (45)$$

$$\text{For } q \geq 0: \quad (46)$$

$$V_N \frac{dS_N}{dt} = q(S_T - S_N) + K_N(S_T - S_N) + F_N S_0 - F_N S_N \quad (47)$$

$$V_T \frac{dS_T}{dt} = q[\gamma S_S + (1 - \gamma)S_{IP} - S_T] + K_S(S_S - S_T) + K_N(S_N - S_T) \\ + F_T S_0 + F_N(\gamma S_S + (1 - \gamma)S_{IP}) + F_S S_S + F_{IP} S_{IP} \quad (48)$$

$$V_S \frac{dS_S}{dt} = q\gamma(S_B - S_S) + K_{IP}(S_{IP} - S_S) + K_S(S_T - S_S) + \eta(S_B - S_S) \\ + F_S S_0 + \gamma F_N(S_B - S_S) - F_S S_S \quad (49)$$

$$V_{IP} \frac{dS_{IP}}{dt} = q(1 - \gamma)(S_B - S_{IP}) + K_{IP}(S_S - S_{IP}) + F_{IP} S_0 \\ + (1 - \gamma)F_N(S_B - S_{IP}) - F_{IP} S_{IP} \quad (50)$$

$$V_B \frac{dS_B}{dt} = q(S_N - S_B) + \eta(S_S - S_B) + F_N(S_N - S_B) \quad (51)$$

$$\text{and for } q < 0: \quad (52)$$

$$V_N \frac{dS_N}{dt} = |q|(S_B - S_N) + K_N(S_T - S_N) + F_N S_0 + (F_T + F_S + F_{IP})S_B \quad (53)$$

$$V_T \frac{dS_T}{dt} = |q|(S_N - S_T) + K_S(S_S - S_T) + K_N(S_N - S_T) + F_T S_0 - F_T S_T \quad (54)$$

$$V_S \frac{dS_S}{dt} = |q|\gamma(S_T - S_S) + K_{IP}(S_{IP} - S_S) + K_S(S_T - S_S) + \eta(S_B - S_S) \\ + F_S S_0 + \gamma F_T(S_T - S_S) - F_S S_S \quad (55)$$

$$V_{IP} \frac{dS_{IP}}{dt} = |q|(1 - \gamma)(S_T - S_{IP}) + K_{IP}(S_S - S_{IP}) + F_{IP} S_0 \\ + (1 - \gamma)F_T(S_T - S_{IP}) - F_{IP} S_{IP} \quad (56)$$

$$V_B \frac{dS_B}{dt} = |q|\gamma S_S + (1 - \gamma)|q|S_{IP} - |q|S_B + \eta(S_S - S_B) + F_S(S_S - S_B) \\ + F_T[\gamma S_S + (1 - \gamma)S_{IP} - S_B] + F_{IP}(S_{IP} - S_B) \quad (57)$$

In contrast to the original model, we do not only demand conservation of salt, but also a conservation of total water volume in each box. This results in two slight differences to the original model:

1. We removed a factor of γ from the second-to-last term of Eq. 11 in (31).

2. F_i describes the flux of freshwater that the ocean surface of box i exchanges with the atmosphere. In the original model, there is a water flux into the boxes with index $i \in \{N, S, T, IP\}$ if $F_i < 0$, which is not removed from the box, while boxes with $F_i > 0$ lose water volume over time.

We therefore added additional fluxes between the boxes. The flux between the boxes N and T remains unchanged as this flux is supposed to describe the strength of the AMOC. Furthermore, we split up the additional flux going from box B into the boxes S and IP by the same factor of γ as used for the AMOC.

We use the same parameter values as given in (31) for the FAMOUS_A simulation, with the exception that in the modified version we use $S_0 = 0.035\text{psu}$ instead of $S_0 = 35\text{psu}$. The reason is that S_0 in the modified model can be interpreted as fresh water salinity (the salinity of the rain) whereas in the original model it represents the average salt water salinity. The original equations are then an approximation of our modified equations. As the modification is very small numerically, all results in this study are very likely to be independent of the model version applied.

Figures

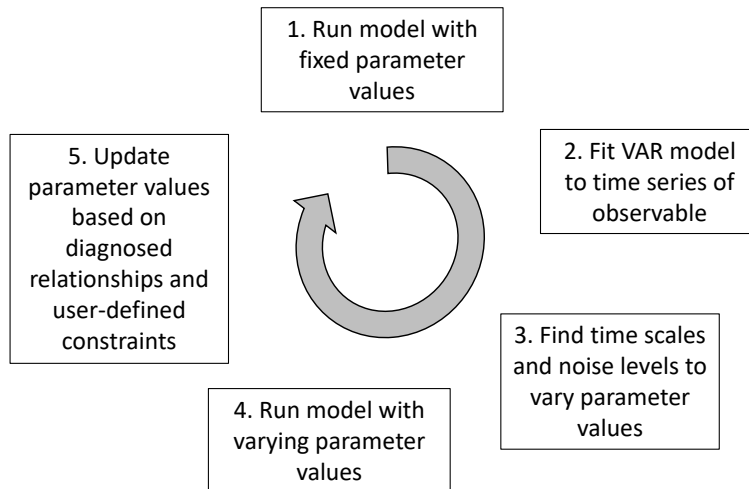


Figure 1: Main steps of our calibration method to automatically shift parameter values that change the stability of a simulated system in a targeted way.

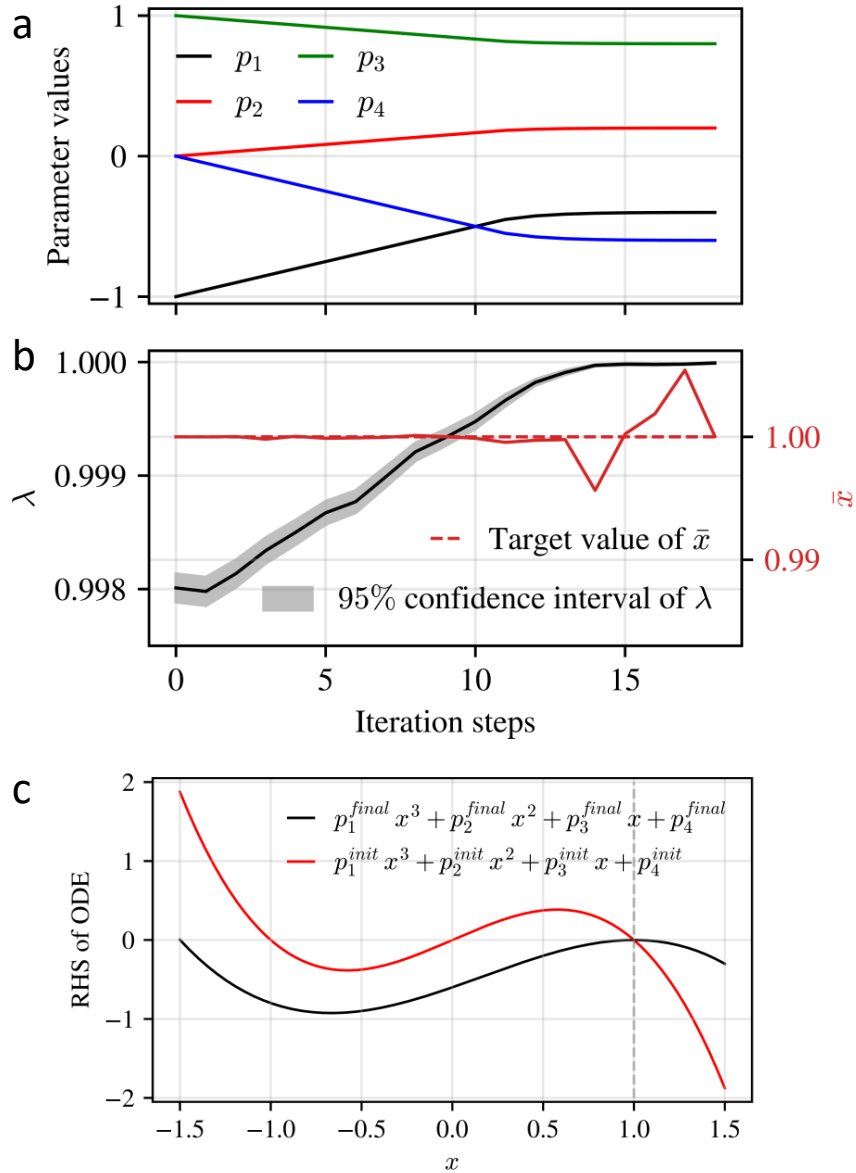


Figure 2: Application of the destabilisation method to the double-well system. a) Evolution of the parameters p_1, \dots, p_4 , and (b) evolution of the Jacobian λ and the mean value \bar{x} of x during the iterative destabilization of the double-well system; note the small y-axis range for the latter. c) The right-hand side (RHS) of equation 16 for the parameters before (red) and after (black) the destabilization of the double-well system. By design, observable x is constrained to stay at $x = 1$ (grey dotted line). The original stable state (negative slope of the red line) eventually merges with an unstable one in a saddle-node bifurcation.

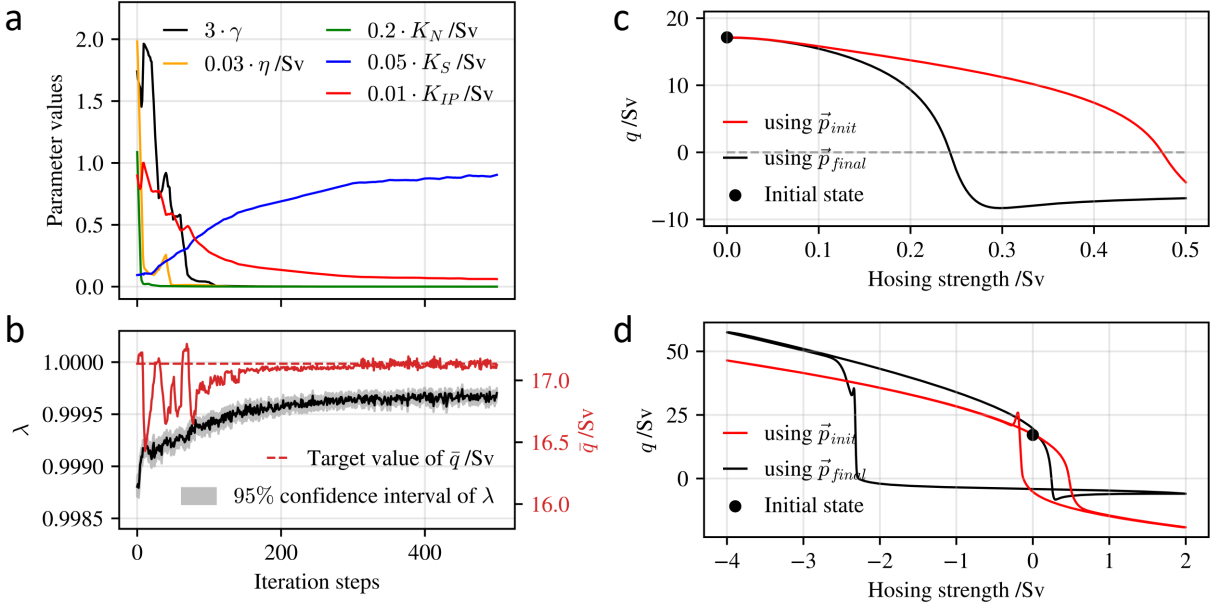


Figure 3: Destabilisation of the 5-box AMOC model with (a) the evolution of the parameters p_1, \dots, p_4 , as well as (b) the Jacobian λ and the mean value \bar{x} of x during the iterative destabilization process. (c) and (d): Hysteresis in the 5-box AMOC model (31) before (red) and after (black) destabilization, when performing the hosing experiment as described in (31) to both systems. (c) Closeup of the hysteresis emphasizing the initial AMOC collapses due to the hosing. (d) Hysteresis curve over the full range of hosing. Note that the horizontal range of hysteresis is strongly increased by the parameter change.

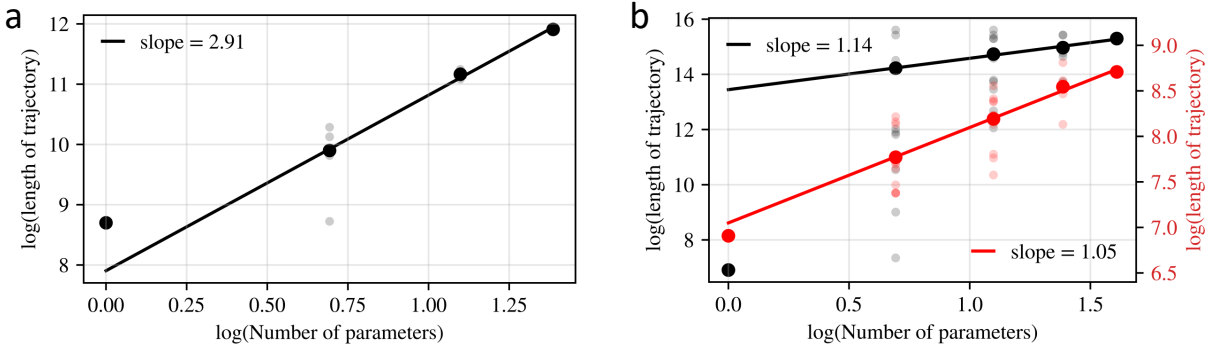


Figure 4: Computational cost of our calibration method to adjust stability for (a) the double well system, (b, black) the box model system, and (b, red) the optimised box model system. Both figures show how the length of the trajectory that is needed in a single iteration step in order to fulfill the accuracy condition (cf. section "Analysing the computational cost of the method"), depends on the number of parameters under consideration. The small transparent data points correspond to (averaged) measurements for a given fixed parameter subset whereas the large data points display the average value taken over all parameter subsets, containing the same number of parameters. By fitting a linear function to the averaged data points in the log-log plot for each system respectively, we infer a polynomial dependence of the trajectory length on the number of parameters. We excluded the data points corresponding to one parameter being varied from the linear fits due to its unique significance for the generation process of the shown data.

References and Notes

1. M. Gelbrecht, A. White, S. Bathiany, N. Boers, Differentiable programming for Earth system modeling. *Geosci. Model Dev.* **16**, 3123–3135 (2023), doi:<https://doi.org/10.5194/gmd-16-3123-2023>.
2. J. M. Gutierrez, A.-M. Treguier, *Annex II: Models. In: Climate Change 2021: The Physical Science Basis. Contribution of Working Group I to the Sixth Assessment Report of the Intergovernmental Panel on Climate Change* (Cambridge University Press, United Kingdom and New York, USA) (2021), doi:10.1017/9781009157896.016.
3. J. Curry, P. Webster, Climate science and the uncertainty monster. *Bulletin of the American Meteorological Society (BAMS)* **92** (12), 1667–1682 (2011), doi:DOI:10.1175/2011BAMS3139.1.
4. D. Stainforth, M. Allen, E. Tredger, L. Smith, Confidence, uncertainty and decision-support relevance in climate predictions. *Phil. Trans. R. Soc. A* **365**, 2145–2161 (2007).
5. C. Shen, A. Appling, P. Gentine, et al., Differentiable modelling to unify machine learning and physical models for geosciences. *Nat Rev Earth Environ* **4**, 552–567 (2023), doi:<https://doi.org/10.1038/s43017-023-00450-9>.
6. T. Mauritsen, et al., Tuning the climate of a global model. *Journal of Advances in Modeling Earth Systems* **4** (3) (2012), doi:<https://doi.org/10.1029/2012MS000154>, <https://agupubs.onlinelibrary.wiley.com/doi/abs/10.1029/2012MS000154>.
7. F. Hourdin, et al., The Art and Science of Climate Model Tuning. *Bulletin of the American Meteorological Society* **98** (3), 589 – 602 (2017), doi:10.1175/BAMS-D-15-00135.1, <https://journals.ametsoc.org/view/journals/bams/98/3/bams-d-15-00135.1.xml>.
8. T. Mauritsen, E. Roeckner, Tuning the MPI-ESM1.2 Global Climate Model to Improve the Match With Instrumental Record Warming by Lowering Its Climate Sensitivity. *Journal of Advances in Modeling Earth Systems* **12**, e2019MS002037 (2020), doi:doi.org/10.1029/2019MS002037.

9. M. Collins, *et al.*, Climate model errors, feedbacks and forcings: a comparison of perturbed physics and multi-model ensembles. *Climate Dynamics* **36**, 1737–1766 (2011).
10. T. M. Lenton, *et al.*, Tipping elements in the Earth’s climate system. *Proceedings of the National Academy of Sciences* **105** (6), 1786–1793 (2008).
11. N. Boers, M. Ghil, T. Stocker, Theoretical and paleoclimatic evidence for abrupt transitions in the Earth system. *Environ. Res. Lett.* **17** (093006) (2022), doi:10.1088/1748-9326/ac8944.
12. D. Chen, *et al.*, *Framing, Context, and Methods*. In: *In Climate Change 2021: The Physical Science Basis. Contribution of Working Group I to the Sixth Assessment Report of the Intergovernmental Panel on Climate Change* (Cambridge University Press, United Kingdom and New York, USA) (2021), doi:10.1017/9781009157896.003.
13. S. Wang, *et al.*, Mechanisms and Impacts of Earth System Tipping Elements. *Reviews of Geophysics* **61** (1), 1–81 (2023), doi:10.1029/2021rg000757.
14. S. Drijfhout, *et al.*, Catalogue of abrupt shifts in Intergovernmental Panel on Climate Change climate models. *Proceedings of the National Academy of Sciences* **112** (43), E5777–E5786 (2015).
15. P. Valdes, Built for stability. *Nature Geoscience* **4**, 414–416 (2011).
16. H. Haken, *Nonequilibrium Phase Transitions and Self-Organization in Physics, Chemistry, and Biology* (Springer Berlin, Heidelberg) (1983).
17. M. Scheffer, *et al.*, Early-warning signals for critical transitions. *Nature* **461** (7260), 53–59 (2009).
18. H. Held, T. Kleinen, Detection of climate system bifurcations by degenerate fingerprinting. *Geophys Res Lett* **31** (2004).
19. N. Boers, M. Rypdal, Critical slowing down suggests that the western Greenland Ice Sheet is close to a tipping point. *PNAS* **118** (21), e2024192118 (2021), doi:https://doi.org/10.1073/pnas.2024192118.

20. N. Boers, Observation-based early-warning signals for a collapse of the Atlantic Meridional Overturning Circulation. *Nature Climate Change* **11** (8), 680–688 (2021), doi:10.1038/s41558-021-01097-4, <http://dx.doi.org/10.1038/s41558-021-01097-4>.
21. C. A. Boulton, T. M. Lenton, N. Boers, Pronounced loss of Amazon rainforest resilience since the early 2000s. *Nature Climate Change* **12** (3), 271–278 (2022).
22. T. Smith, D. Traxl, N. Boers, Empirical evidence for recent global shifts in vegetation resilience. *Nature Climate Change* **12** (5), 477–484 (2022).
23. N. Bochow, N. Boers, The South American monsoon approaches a critical transition in response to deforestation. *Science Advances* **9** (40), eadd9973 (2023).
24. T. Kleinen, H. Held, G. Petschel-Held, The potential role of spectral properties in detecting thresholds in the Earth system: application to the thermohaline circulation. *Ocean Dynamics* **53**, 53–63 (2003), doi:<https://doi.org/10.1007/s10236-002-0023-6>.
25. C. Boulton, L. Allison, T. Lenton, Early warning signals of Atlantic Meridional Overturning Circulation collapse in a fully coupled climate model. *Nat Commun* **5**, 5752 (2014).
26. S. Bathiany, M. Claussen, K. Fraedrich, Detecting hotspots of atmosphere–vegetation interaction via slowing down — Part 1: A stochastic approach. *Earth Syst Dynam* **4**, 63–78 (2013), doi:<https://doi.org/10.5194/esd-4-63-2013>.
27. S. Bathiany, M. Claussen, K. Fraedrich, Detecting hotspots of atmosphere–vegetation interaction via slowing down — Part 2: Application to a global climate model. *Earth Syst Dynam* **4**, 79–93 (2013), doi:<https://doi.org/10.5194/esd-4-79-2013>.
28. E. Weinans, *et al.*, Finding the direction of lowest resilience in multivariate complex systems. *J. R. Soc. Interface* **16**, 20190629 (2019), doi:<http://dx.doi.org/10.1098/rsif.2019.0629>.
29. K. J. Astroem, B. Wittenmark, On Self Tuning Regulators. *Automatica* **9**, 185–199 (1973).
30. T. Baumeister, S. Brunton, J. Kutz, Deep learning and model predictive control for self-tuning mode-locked lasers. *Journal of the Optical Society of America B* **35** (3), 617–626 (2018).

31. R. A. Wood, J. M. Rodríguez, R. S. Smith, L. C. Jackson, E. Hawkins, Observable, low-order dynamical controls on thresholds of the Atlantic meridional overturning circulation. *Climate Dynamics* **53** (11), 6815–6834 (2019), doi:10.1007/s00382-019-04956-1, <https://doi.org/10.1007/s00382-019-04956-1>.
32. E. L. McDonagh, *et al.*, Continuous Estimate of Atlantic Oceanic Freshwater Flux at 26.5°N. *Journal of Climate* **28**, 8888–8906 (2015), doi:10.1175/JCLI-D-14-00519.1.
33. L. C. Jackson, R. S. Smith, R. A. Wood, Ocean and atmosphere feedbacks affecting AMOC hysteresis in a GCM. *Climate Dynamics* **49**, 173–191 (2017), doi:10.1007/s00382-016-3336-8.
34. N. Urban, T. Fricker, A comparison of Latin hypercube and grid ensemble designs for the multivariate emulation of an Earth system model. *Computers & Geosciences* **36** (6), 746–755 (2010), doi:<https://doi.org/10.1016/j.cageo.2009.11.004>.
35. D. B. Williamson, A. T. Blaker, B. Sinha, Tuning without over-tuning: parametric uncertainty quantification for the NEMO ocean model. *Geosci. Model Dev* **10**, 1789—1816 (2017).
36. S. Peatier, B. M. Sanderson, L. Terray, R. Roehrig, Investigating parametric dependence of climate feedbacks in the atmospheric component of CNRM-CM6-1. *Geophysical Research Letters* **49**, – (2022), doi:10.1029/2021GL095084.
37. F. Berkenkamp, A. Krause, A. P. Schoellig, Bayesian optimization with safety constraints: safe and automatic parameter tuning in robotics. *Machine Learning* **112**, 3713–3747 (2023), doi:<https://doi.org/10.1007/s10994-021-06019-1>.
38. F. Hourdin, *et al.*, Toward machine-assisted tuning avoiding the underestimation of uncertainty in climate change projections. *Science Advances* **9**, eadf2758 (2023).
39. D. McNeall, *et al.*, The impact of structural error on parameter constraint in a climate model. *Earth System Dynamics* **7**, 917–935 (2016), doi:10.5194/esd-7-917-2016.
40. M. e. a. Claussen, Earth system models of intermediate complexity: closing the gap in the spectrum of climate system models. *Climate Dynamics* **18**, 579–586 (2002), doi:10.1007/s00382-001-0200-1.

41. H. Lütkepohl, *New introduction to multiple time series analysis* (Springer, Berlin [u.a.]) (2005), http://gso.gbv.de/DB=2.1/CMD?ACT=SRCHA&SRT=YOP&IKT=1016&TRM=ppn+366296310&sourceid=fbw_bibsonomy.
42. H. Alkhayuon, P. Ashwin, L. Jackson, C. Quinn, R. Wood, Basin bifurcations, oscillatory instability and rate-induced thresholds for Atlantic meridional overturning circulation in a global oceanic box model. *Proc. R. Soc. A* **475**, 20190051 (2019), <http://dx.doi.org/10.1098/rspa.2019.0051>.

Acknowledgments

Funding: This is ClimTip contribution #4; the ClimTip project has received funding from the European Union's Horizon Europe research and innovation programme under grant agreement No. 101137601. N.B. and S.B. acknowledge funding by the Volkswagen foundation.

Author contributions: N.B. and S.B. defined the research goal, D.P. designed the implementation and execution of the method, D.P. and R.W. implemented the 5-box model, D.P. and S.B. wrote a first draft of the manuscript, and all authors wrote the final version of the paper.

Competing interests: There are no competing interests to declare.

Data and materials availability: Julia code implementing our method as well as the two numerical models used in this study can be found at https://github.com/DanielJonathanPals/parametrization_stability.

Supplementary materials

Supplementary Materials for
Targeted calibration to adjust stability biases in
non-differentiable complex system models

Daniel Pals^{1*}, Sebastian Bathiany^{1,2}, Richard Wood³, Niklas Boers^{1,2,4*}

*Corresponding authors. E-mail: daniel.pals@tum.de and n.boers@tum.de

This PDF file includes:

Supplementary Methods

Supplementary Methods

Evaluation of the VAR(1) model

As an additional suggestion, we propose to evaluate the accuracy of the VAR approximation by comparing forecasts from the original model and the approximated VAR model, defining some expected error bounds. Assume that we have an estimated VAR model and (\vec{z}_t^{new}) and (\vec{y}_t^{new}) represent some additional data not used to estimate the model. Then the one-step ahead prediction $\hat{z}_t^{new}(1)$ of \vec{z}_{t+1}^{new} is given by $\vec{v} + A\vec{y}_t^{new}$. As similarly presented in section 3.5 in (41), the covariance matrix of this one-step prediction is given by

$$\Sigma_z(1) = \frac{T + d_y + 1}{T} \Sigma_\varepsilon \quad (\text{S1})$$

Here, Σ_ε is the covariance matrix of the offsets $\vec{\varepsilon}$, which can be estimated as given in equation 34, and T is the length of the data series used to estimate the model.

A possible procedure to test the model using one-step forecasts could be the following: Assume we have n validation samples available. Then for each $i \in \{1, \dots, n\}$ the one step forecast $\hat{z}_i^{new}(1)$ is computed as

$$\hat{z}_i^{new}(1) = BY_i^{new} = \vec{v} + A\vec{y}_i^{new} \quad (\text{S2})$$

We can then use this for each i

$$(\vec{z}_i^{new} - \hat{z}_{i-1}^{new}(1))' \Sigma_z(1)^{-1} (\vec{z}_i^{new} - \hat{z}_{i-1}^{new}(1)) \sim \chi^2(d_z) \quad (\text{S3})$$

If we now pick a random subset $A \subseteq \{1, \dots, n\}$ of cardinality $|A| \ll n$ and for n sufficiently large, we can assume that the corresponding one-step forecasts are uncorrelated. This leads to

$$\sum_{i \in A} (\vec{z}_i^{new} - \hat{z}_{i-1}^{new}(1))' \Sigma_z(1)^{-1} (\vec{z}_i^{new} - \hat{z}_{i-1}^{new}(1)) \sim \chi^2(d_z | A) \quad (\text{S4})$$

which is a criterion that can be tested.

Testing for whiteness of the VAR residuals

Here we suggest a hypothesis test for quantifying the whiteness of the residuals (see section 4.4 in (41)). This means testing whether the autocorrelation of the series (u_t) vanishes. We set up a

model

$$\varepsilon_t = D_1\varepsilon_{t-1} + \dots + D_h\varepsilon_{t-h} + e_t \quad (\text{S5})$$

with e_t as error terms and test the hypothesis $H_0 : D_1 = \dots = D_h = 0$ against $H_1 : D_j \neq 0$ for at least one $j \in \{1, \dots, h\}$.

Using a Lagrange Multiplier Test, we first define

$$\hat{E} = Z - BY \quad (\text{S6})$$

$$F_i = \begin{bmatrix} 0_{(i \times T-i)} & 0_{(i \times i)} \\ \text{Id}_{T-i} & 0_{(T-i \times i)} \end{bmatrix} \quad (\text{S7})$$

$$F = (F_1, \dots, F_h) \quad (\text{S8})$$

$$\hat{C} = (\text{Id}_h \otimes \hat{E})F' \quad (\text{S9})$$

$$e = (e_1, \dots, e_T) \quad (\text{S10})$$

$$D = (D_1, \dots, D_h) \quad (\text{S11})$$

using the same notation as introduced in Materials and Methods, VAR(1) model estimation. As described in Appendix C.7 or section 4.4.4 in (41), it can be shown that the hypothesis test as described above is equivalent to testing whether

$$\lambda_{LM}(h) = \text{vec}(\hat{E}\hat{E}')' \left([\hat{E}\hat{E}' - \hat{E}Y'(YY')^{-1}Y\hat{E}']^{-1} \otimes \hat{\Sigma}_\varepsilon^{-1} \right) \text{vec}(\hat{E}\hat{E}') \quad (\text{S12})$$

is compatible with a $\chi^2(hd_x^2)$ distribution. To this end, we use that we know the mean value and variance of the χ^2 distribution, which allows us to define a confidence interval where we can test whether or not λ_{LM} lies inside it or not.

Improvement of VAR estimation by denoising

In order to potentially increase the accuracy of the VAR estimation with fixed parameters, which is also needed for fixed parameter values (step 2 of our recipe above), one can again exploit the fact that we know the noise values $\vec{u}_t^{(x)}$ used as offsets for computing the trajectories of the system variables \vec{x}_t . To this end, we first record the trajectory (including noise) of system variables (\vec{x}_t),

which can then be used to compute the corresponding observable trajectory (\vec{o}_t) using f_o . We then compute a second trajectory (\tilde{o}_t) defined by

$$\tilde{o}_t = f_o(f_p(\vec{x}_{t-1}, \vec{p}_{init}), \vec{p}_{init}), \quad (\text{S13})$$

i.e. we use the same trajectory but remove the noise in each step. Note that we are considering the case of fixed parameters, which is the reason why we use $\vec{p} = \vec{p}_{init}$ as second argument for f_o and f_p . If we now estimate the VAR model with $\vec{z}_t = \tilde{o}_t$ and $\vec{y}_t = \vec{o}_t$ using the procedure and the notation from Materials and Methods (VAR(1) model estimation), we maintain the benefits of forcing our system with additive white noise – i.e. forcing the system out of equilibrium and ”coarse graining” the Jacobian at the equilibrium to a desired scale – but remove the noise from the VAR model estimation. We note that this does not always increase the quality of the VAR model estimation even in the case of simple linear dynamical systems, since $f_o(\cdot, \vec{p})$ is not injective in general. This means that multiple configurations of the system variables could lead to the same value for the observable, but the values of the observable in the next time step might differ. In cases where this effect plays a dominant role, the benefit of cutting out the noise forcing might be negligible. In the case of the 5-box model, we found that including the noise correction for the fixed-parameter VAR model only has a negligible effect on the quality of the VAR model estimation, so we did not apply it for simplicity and for the sake of cutting down the computational costs.